The Journal of Chemical Physics ARTICLE scitation.org/journal/jcp

PASP: Property analysis and simulation package for materials

Cite as: J. Chem. Phys. 154, 114103 (2021); doi: 10.1063/5.0043703
Submitted: 11 January 2021 • Accepted: 22 February 2021 •
Published Online: 15 March 2021

Feng Lou,[1] X. Y. Li,[1] J. Y. Ji,[1] H. Y. Yu,[1] J. S. Feng,[1] X. G. Gong,[1,2] and H. J. Xiang[1,2,a)]

AFFILIATIONS

[1]Key Laboratory of Computational Physical Sciences (Ministry of Education), State Key Laboratory of Surface Physics, and Department of Physics, Fudan University, Shanghai 200433, China
[2]Shanghai Qizhi Institution, Shanghai 200232, China

Note: This paper is part of the JCP Special Topic on Computational Materials Discovery.
[a)]**Author to whom correspondence should be addressed:** hxiang@fudan.edu.cn

ABSTRACT

We have developed a software package, namely, PASP (Property Analysis and Simulation Package for materials), to analyze the structural, electronic, magnetic, and thermodynamic properties of complex condensed matter systems. Our package integrates several functionalities including symmetry analysis, global structure searching methods, effective Hamiltonian methods, and Monte Carlo simulation methods. In conjunction with first-principles calculations, PASP has been successfully applied to diverse physical systems. In this paper, we give a brief introduction to its main features and underlying theoretical formulism. Some typical applications are provided to demonstrate the usefulness, high efficiency, and reliability of PASP. We expect that further developments will make PASP a general-purpose tool for material simulation and property calculation of condensed matters.

I. INTRODUCTION

Traditionally, experimental studies on new materials are a long and costly process due to the huge amount of trials and errors in synthesizing and testing. At some particular circumstances, e.g., high pressure or high magnetic field, these experiments may be not accessible. As a comparison, computational analysis is a powerful tool to predict material properties and design new functional materials without these limitations. Recent advances in first-principles theory and computing power have enabled us to perform computational studies with low cost.

In many interesting condensed matter systems (e.g., transition metal oxides), the presence of multiple degrees of freedoms (e.g., spin, orbital, charge, and lattice) and their interplay lead to rich exotic phenomena (such as colossal magnetoresistance, multiferroicity, insulator-metal transition, and quantum spin liquid state). Understanding the coupling mechanisms between these degrees of freedoms is not only of fundamental importance but will also speed up practical applications of these complex condensed matter systems. Although first-principles calculation packages were found to be very useful for investigating complex condensed matter systems, they have some insurmountable limitations. For instance, a direct use of the first-principles calculation packages for computing the thermodynamic and/or kinetic properties of complex condensed matter systems is forbidden due to the huge computational amount. Besides, usually the first-principles calculation packages give the final result (i.e., electric polarization) of a physical property, and they do not provide a clear physical picture without further comprehensive analysis.

To facilitate the computational studies on complex condensed matter systems, we have developed a software package called PASP (Property Analysis and Simulation Package for materials). On the basis of first-principles calculations, PASP is able to compute the thermodynamic properties of complex condensed matter systems and provide insight into the microscopic mechanisms of the coupling between multiple degrees of freedoms. Our current PASP package includes several functionalities. To be more specific, we implemented symmetry and group theory analysis, which is used extensively by the other modules. PASP includes a global structure searching module that can be adopted to predict the quantum ground state of complex systems in combination with first-principles calculation packages. Various effective Hamiltonian

methods are implemented in PASP. The tight binding method is implemented to understand not only the electronic structure but also the related properties (e.g., magnetic exchange coupling, ferroelectric instability, and magnetoelectric coupling). The spin Hamiltonian and effective Hamiltonian for ferroelectrics and multiferroics are also implemented. PASP also provides methods for constructing these Hamiltonians on the basis of first-principles calculations. These Hamiltonians can either be of a polynomial form or a machine-learning type (e.g., neural network). The parallel tempering Monte Carlo (PTMC) simulations with these effective Hamiltonians can efficiently compute the thermodynamic properties of these complex condensed matter systems. Because of these functional features, PASP can be widely used to predict the atomic structures, compute the material properties, and simulate the material behaviors. Different from the existing well-known packages[1–3] that implement one main specific functionality, PASP has many functional features in a single package. This unique characteristic makes PASP convenient for both users and developers. In the following, we discuss the methodologies of these functional features (see Fig. 1) and the usage of PASP with several applications.

II. FEATURES AND METHODOLOGIES

PASP currently implements many functional features. In this section, we will describe the main methodologies of these functional features.

A. Symmetry and group theory analysis

Symmetry and group theory analysis is fundamental in the study of condensed matter systems.[4] The determination of the point group and space group of crystals is the foundation of symmetry analysis. Besides finding the symmetry operations of a structure, our PASP package includes some other symmetry analysis functions. In this part, we will first discuss the main procedure of determining the point group and space group. Then, we will present an important application of symmetry analysis to determine the irreducible representation (IR) of Bloch wave functions of crystals.

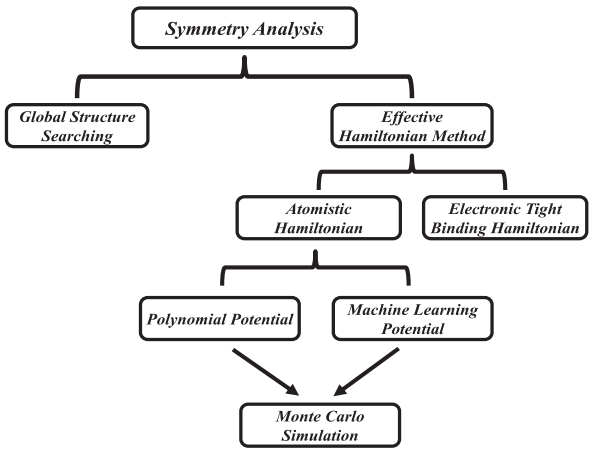

FIG. 1. Schematic illustration of functional features of our Property Analysis and Simulation Package for materials (PASP). The symmetry analysis is the foundation of PASP. We implement the effective atomistic Hamiltonian method and the electronic tight binding method. The effective atomistic Hamiltonian has two different methodologies, that is, polynomial potential and machine learning potential, which can both be used in conjunction with the Monte Carlo simulations.

Our algorithm to identify the space group and point group of crystals is based on the following key observation: for the operation $\{\hat{R}|t\}$ of the space group G, the rotational part $\hat{R}$ must belong to the point group G_L of the Bravais lattice. First, we determine the type of Bravais lattice by the following two steps: (i) read the crystallographic vectors and transform them to the standard settings and (ii) calculate the lengths of the three axes and cosines between the axes. Now, one can determine the Bravais lattice according to the definitions of 14 three-dimensional Bravais lattices. Second, we set up all space group operators by the following steps: (i) set up G_L in the standard settings according to the Bravais lattice and (ii) for all point group operators $\hat{R}$ in G_L, find out operations $\{\hat{R}|t\}$ (where t is an appropriate fractional translation associated with $\hat{R}$) that keep the structure invariant. All these $\{\hat{R}|t\}$ operations form the space group G. The point group G_0 can be obtained by considering the rotational part $\hat{R}$ of all operations $\{\hat{R}|t\}$ of the space group G. In this way, one can identify the space group and point group of a crystal.

The IR of Bloch wave functions is useful in the study of many material properties. For example, the IR of the wave function helps deduce the topological properties of materials.[5] For an allowed optical transition, the direct product of the IRs of the initial state, the final state, and the transition operator must contain the fully symmetric irreducible representation. In another context, the k.p model Hamiltonian can be derived with an invariant method using the IR of the electronic states. Thus, we implement a method to determine the IRs of Bloch wave functions.

The wave functions can be written as $\psi_{b_i}(\vec{\boldsymbol{k}},\vec{\boldsymbol{r}})(i=1,\ldots,d)$, where b_i is the band index, d is the degeneracy of this band manifold, and $\vec{\boldsymbol{k}}$ is a wave vector in the Brillouin zone of the reciprocal space. These wave functions form a set of basis functions for a d-dimensional representation Γ of the little group $G_{\boldsymbol{k}}$ (a subgroup of G whose elements $\{\hat{R}|t\}$ satisfy $\hat{R}\vec{\boldsymbol{k}}=\vec{\boldsymbol{k}}+\vec{\boldsymbol{Q}}$, where $\vec{\boldsymbol{Q}}$ is a reciprocal lattice vector): $\forall \hat{P}_{\boldsymbol{k}} \in G_{\boldsymbol{k}}$, $\hat{P}_{\boldsymbol{k}}\Psi(\vec{\boldsymbol{k}},\vec{\boldsymbol{r}})=D_\Gamma(\hat{P}_{\boldsymbol{k}})\Psi(\vec{\boldsymbol{k}},\vec{\boldsymbol{r}})$, where $\Psi(\vec{\boldsymbol{k}},\vec{\boldsymbol{r}})=\left(\psi_{b_1}(\vec{\boldsymbol{k}},\vec{\boldsymbol{r}}),\ldots,\psi_{b_d}(\vec{\boldsymbol{k}},\vec{\boldsymbol{r}})\right)^T$ and $D_\Gamma(\hat{P}_{\boldsymbol{k}})$ is the d-dimensional matrix of representation Γ spanned by $\psi_{b_i}(\vec{\boldsymbol{k}},\vec{\boldsymbol{r}})(i=1,\ldots,d)$. By computing $\hat{P}_{\boldsymbol{k}}\Psi(\vec{\boldsymbol{k}},\vec{\boldsymbol{r}})$, one can easily obtain the representation matrix of $D_\Gamma(\hat{P}_{\boldsymbol{k}})$. By comparing the traces of $D_\Gamma(\hat{P}_{\boldsymbol{k}})$ with the character table of $G_{\boldsymbol{k}}$, one can determine the IR spanned by $\psi_{b_i}(\vec{\boldsymbol{k}},\vec{\boldsymbol{r}})$ $(i=1,\ldots,d)$.

In the above discussions, we do not take spin–orbit coupling (SOC) into consideration. In that case, we can consider only the spatial part of the wave function. When considering the SOC effect on the electronic structure of the nonmagnetic system, we must deal with the spinor wave function, that is,

$$\psi_{b_i}(\vec{\boldsymbol{k}},\vec{\boldsymbol{r}})=\begin{pmatrix}\psi_{b_i,\uparrow}(\vec{\boldsymbol{k}},\vec{\boldsymbol{r}})\\ \psi_{b_i,\downarrow}(\vec{\boldsymbol{k}},\vec{\boldsymbol{r}})\end{pmatrix}=\psi_{b_i,\uparrow}(\vec{\boldsymbol{k}},\vec{\boldsymbol{r}})\begin{pmatrix}1\\0\end{pmatrix}+\psi_{b_i,\downarrow}(\vec{\boldsymbol{k}},\vec{\boldsymbol{r}})\begin{pmatrix}0\\1\end{pmatrix},\quad (i=1,\ldots,d).$$

To describe the symmetry property of spinor wave functions, we adopt a double space group in which the element contains not only the usual three-dimensional space group operation but also a

two-dimensional rotation $\hat{P}_{k,s}$ in the spin space. That is,

$$\hat{P}_k\psi_{b_i}(\vec{k},\vec{r}) = \hat{P}_k\begin{pmatrix}\psi_{b_i,\uparrow}(\vec{k},\vec{r})\\ \psi_{b_i,\downarrow}(\vec{k},\vec{r})\end{pmatrix} = \hat{P}_{k,s}\begin{pmatrix}\{\hat{R}_k|\vec{t}\}\psi_{b_i,\uparrow}(\vec{k},\vec{r})\\ \{\hat{R}_k|\vec{t}\}\psi_{b_i,\downarrow}(\vec{k},\vec{r})\end{pmatrix}$$
$$= \hat{P}_{k,s}\begin{pmatrix}\psi''_{b_i,\uparrow}(\vec{k},\vec{r})\\ \psi''_{b_i,\downarrow}(\vec{k},\vec{r})\end{pmatrix} = \begin{pmatrix}a\psi''_{b_i,\uparrow}(\vec{k},\vec{r}) + b\psi''_{b_i},\downarrow(\vec{k},\vec{r})\\ -\bar{b}\psi''_{b_i,\uparrow}(\vec{k},\vec{r}) + \bar{a}\psi''_{b_i,\downarrow}(\vec{k},\vec{r})\end{pmatrix},$$

where the two-dimensional unitary matrix $\hat{P}_{k,s}$ can be written as $\hat{P}_{k,s} = \begin{pmatrix}a & b\\ -\bar{b} & \bar{a}\end{pmatrix}$. Note that the SU(2) matrix $\hat{P}_{k,s}$ can be computed from the 3×3 matrix representation of $\hat{R}_k$. After obtaining the transformed spinor wave function, one can obtain the IR of spinor wave functions in the way similar to the non-SOC case. Generally speaking, our method can give the IR for the Bloch wave function, no matter $\vec{k}$ lies at the boundary of the Brillouin zone or not, no matter the space group is symmorphic or non-symmorphic, and no matter SOC is considered or not. Our method has been applied to investigate the IRs of electronic states of bulk symmorphic GaAs, two-dimensional non-symmorphic SnTe, and two-dimensional symmorphic FeB_2.[6,7]

B. Global structure searching

Determining the crystal structure is fundamental in material science due to the close relationship between structure and properties. Therefore, prediction of the crystal structure is an important task not only in designing new functional material but also in understanding the physical properties. The most simple way to search the ground state structure is generating random structures to calculate their total energies, called *ab initio* random structure searching (AIRSS).[8] However, it may be inefficient for systems containing a large number of atoms. In the past, some other algorithms were proposed to predict the ground state structure.[1,2,9–12] In our package, we implemented the basin-hopping method[13] and genetic algorithms (GA) to predict the structures of clusters,[14] 2D and 3D crystals, and interfaces.[15] Here, we will mainly discuss the genetic algorithm (GA), which is one of the most popular evolutionary algorithm inspired by the natural heredity and mutation. It is worth noting that we recently develop the GA-based global optimization approach that considers explicitly the magnetic degree of freedom,[16] which was usually disregarded in other structure prediction packages. In the following discussion, we take the magnetic system as an example to discuss our methodology.

The flowchart of our global structure searching method is shown in Fig. 2(a). There are four main steps in our method: (i) generate the initial structures, (ii) locally optimize by first-principles calculations, (iii) sort the structures and remove duplicates, and (iv) generate child structures by the genetic algorithm. After the GA evolution in step (iv), we return to step (ii) until we reach the stopping criterion.

The fully random initialization of the first generation will result in poor efficiency of finding the global minimum. Therefore, we generate the initial structures by randomly choosing one of the 230 space groups for bulk (80 for two-dimensional systems). Once a particular space group **G** is selected, the lattice parameters and atomic coordinates are generated according to the symmetry operations and Wyckoff positions. This method is named as the full genetic algorithm (FGA). The FGA is powerful in finding the ground state structure without giving any prior structural information. However,

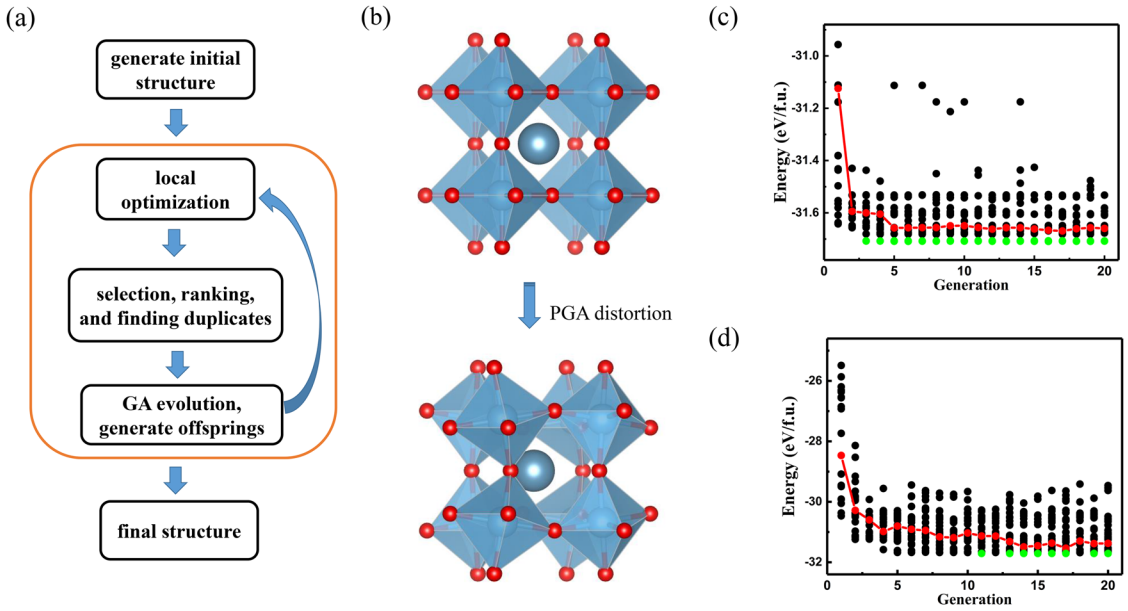

FIG. 2. The global structure searching method. (a) The flowchart of the GA method. (b) Take cubic perovskite as an example to illustrate the PGA method. (c) The evolution of total energies during FGA iterations. (d) The evolution of total energies during PGA iterations. The black dot denotes the individual structure after the local optimization, the green dot highlights the ground state configuration, and the red dot signifies the average energy at each generation.

in some specific class of materials such as transition metal perovskite oxides, we have the basic geometrical framework, and the ground state is the distorted child structure of the high symmetry parent state. Therefore, as shown in Fig. 2(b), we propose another way to generate the initial structures named perturbation genetic algorithm (PGA). In this case, we first randomly select a subgroup **G** of the high symmetry space group $\mathbf{G_p}$ (e.g., cubic $Pm\bar{3}m$ for perovskite oxide). Then, we generate a random structure with the space group **G** by the following procedures: (1) give some small perturbations (atomic displacements and strains) on the parent structure $\mathbf{G_p}$ and (2) symmetrize the distorted structure with the symmetry of **G**. In this way, the new structure is distorted from the parent structure $\mathbf{G_p}$ and has the space symmetry of **G**. Now, with the FGA or PGA method, we can obtain the random structure with the specific space group **G**. To incorporate the magnetic configuration, we randomly choose a magnetic space group that is compatible with the given space group **G**. The spin directions of the magnetic ions are then set according to the magnetic space group. For the ions with variable valence states (e.g., Co^{2+} and Co^{3+}), the spin values can vary accordingly.

During the local optimization of structures, we use the first-principles calculations to relax the structures and calculate their total energies. For the system with magnetic ions, we should optimize the spin moments as well. To increase the diversity of the structures, one needs to sort the structures and remove the duplicates. When evaluating the similarity of two magnetic structures, we first adopt the bond characterization matrix[1] to distinguish the geometrical configuration. If they are close to each other, we further check whether they have similar magnetic configuration. By this way, we can remove the duplicates with almost the same geometrical structure and magnetic configuration.

After sorting the structures, we use the GA method to generate child structures. The basic idea of our GA method is to evolve the parent structures using variation operators, which include crossover (creating the child structure from the slices of two or more parent structures), mutation (creating the child structure by giving the distortion on a single parent), and permutation (creating the child structure by exchanging the positions between two different atoms). For our traditional FGA method, we perform the crossover process with cut-and-splice operation on the atomic positions. While in our PGA method, we introduce an additional mating operation besides the traditional cut-and-splice method proposed by Deaven and Ho.[17] Since many structures can be considered as the child structures with distortions on the high symmetry structure, we can treat these distortions as the superposition of different modes [e.g., the octahedron rotation and ferroelectric (FE) displacement in the $R3c$ phase of $BiFeO_3$]. As a consequence, we propose the following mating operation as $X_{child} = X_{orig} + (X_{father} - X_{orig}) + \lambda(X_{mother} - X_{orig})$, where X_{child} represents the child structure, X_{orig} represents the high symmetry structure, X_{father} and X_{mother} represent the parent structures, and the constant λ is randomly chosen to be 1 or −1 so as to take the sum or difference between these two distortions. For the mutation process, we apply distortions to the lattice parameters and atomic positions. For the permutations, we exchange the positions of two different atoms. When we generate the child structures, we usually have the possibility of 75%, 20%, and 5% to perform crossover, mutation, and permutation, respectively. In the past, our global structure searching method has been used to predict many systems and some of them have been confirmed by experiments.[11,14–16,18–24]

C. Effective Hamiltonian methods

The first-principles calculation is accurate in computing the physical properties of condensed matter systems. However, it is usually restricted to the computation of zero-temperature properties of small systems. The effective Hamiltonian method is proposed to deal with large-scale systems, finite-temperature properties, and/or effects of external fields. Not only it is much more efficient than first-principles calculations, but also it provides a clearer physical picture.

The effective Hamiltonian method can be applied to the study of many physical systems. In our package, we implement several different types of effective Hamiltonian methods. First, at the electronic level, we adopt the tight binding (TB) model Hamiltonian to describe qualitatively the electronic structure. It can help us understand not only the electronic properties but also the physical mechanism of magnetic exchange coupling, ferroelectric instability, and magnetoelectric coupling. Apart from the electronic TB method, we develop the effective atomistic Hamiltonian method to treat the atomic displacement, spin, alloy, and/or strain in a systematic way. The general approach to obtain the effective atomistic Hamiltonian is based on the following four steps: (i) choose the freedoms (e.g., atomic displacement and spin) according to the nature of the physical system, (ii) perform the Taylor expression of these freedoms from low to high orders and from near to far interactions, (iii) use the group theory to find the appropriate interacting forms of these dynamic variables that form the basis of the invariant representation of a given point group, and (iv) fit the undetermined parameters of these energy functions. Then, we discuss the effective magnetic Hamiltonian. We introduce our four-state method to evaluate the exchange interaction parameters. After that, we discuss the effective Hamiltonian for ferroelectrics. Now, we discuss the effective Hamiltonian for multiferroics. For complicated systems, the effective Hamiltonian can be very complicated, and it can be difficult to obtain the reliable interacting parameters. To address this issue, we put forward a machine learning (ML) approach to construct realistic effective Hamiltonians, which can select out the important interactions among a set of possible terms and determine the values of these parameters. Sometimes, the polynomial form may fail to describe the intricate couplings between multiple degrees of freedoms. Therefore, we put forward the effective Hamiltonian method in terms of the machine learning potential form (e.g., neural network). After obtaining the effective Hamiltonian, we can use Monte Carlo simulation to investigate the ground state and simulate the temperature-dependent phase transition.

1. Tight binding Hamiltonian

The empirical TB method is a useful tool to describe qualitatively the electronic structures of materials. For example, the TB method was adopted to understand deeply the electronic structures of 2D graphene[25–27] and monolayer MoS_2.[27–29] In the TB method, one essentially parameterizes the Hamiltonian matrix elements associated with localized atomic-like basis orbitals and diagonalizes the Hamiltonian matrix to compute the eigenvalues and eigenvectors

of the electronic wave functions. The TB method is especially simple and elegant in the second quantization notation, which can be applied to both the extended system and cluster.[30–32] Here, we discuss the TB model in real space, which can be transferred to momentum space by the Fourier transform in the case of periodic systems. Using the atomic orbitals $|\varphi_{R_{i\alpha}}\rangle$ as the orthogonal basis (the orthogonal relation reads $\delta_{i\alpha,j\beta} = \langle\varphi_{i\alpha}|\varphi_{j\beta}\rangle$), the second quantized Hamiltonian for spin-less particles can be written as

$$\widehat{H}_0 = \sum_{R,i\alpha} \epsilon_{Ri\alpha}\hat{a}^{+}_{i\alpha}(\boldsymbol{R})\hat{a}_{i\alpha}(\boldsymbol{R}) + \sum_{R,i\alpha;R'j\beta} t_{Ri\alpha,R'j\beta}\hat{a}^{+}_{i\alpha}(\boldsymbol{R})\hat{a}_{j\beta}(\boldsymbol{R'}),$$

where $\hat{a}^{+}_{i\alpha}(\boldsymbol{R})/\hat{a}_{i\alpha}(\boldsymbol{R})$ creates/annihilates an electron of α orbital of the ith atom in the unit cell $\boldsymbol{R}$, the on-site energy $\epsilon_{Ri\alpha} = \langle\varphi_{Ri\alpha}|\widehat{H}|\varphi_{Ri\alpha}\rangle$ includes the effect of crystal field splitting, and the hopping energy $t_{Ri\alpha,R'j\beta} = \langle\varphi_{Ri\alpha}|\widehat{H}|\varphi_{R'j\beta}\rangle$ involves both two-center and three-center contributions. Usually, the three-center hopping energy is negligible since it is smaller than the two-center energy term. The two-center hopping energy can be conveniently expressed as Slater–Koster integrals.[30] One can have on-site energies and hopping energies by fitting the experimental results or first-principles calculations. Alternatively, the dependence of the hopping parameters on the atomic environment can be evaluated as proposed by Harrison.[33] For instance, $t_{ss\sigma}$, $t_{sp\sigma}$, $t_{pp\sigma}$, and $t_{pp\pi}$ are proportional to $1/d^2$. $t_{pd\sigma}$ and $t_{pd\pi}$ are proportional to $1/d^4$. $t_{dd\sigma}$, $t_{dd\pi}$, and $t_{dd\delta}$ are proportional to $1/d^5$. Here, d is the distance between two atoms.

It is easy to diagonalize the Hamiltonian to achieve the energy spectrum and density of states in real and momentum space. Note that if the basis is not orthogonal, we need to consider the overlap integrals $S_{i\alpha,j\beta} = \langle\varphi_{Ri\alpha}|\varphi_{Rj\beta}\rangle$ and then solve the generalized eigenvalue equation. So far, we considered the minimal TB model suitable for spin-less particles. When the SOC is important, we can generalize the minimal TB formalism to the case of spinors by doubling each TB orbitals (i.e., up-spin and down-spin orbitals). Usually, the relativistic SOC effect can be expressed as $\widehat{H}_{soc} = \sum_i \lambda_i \hat{\boldsymbol{l}}\cdot\hat{\mathbf{s}}$, where λ_i is the SOC strength for the ith atom, $\hat{\boldsymbol{l}}$ is the angular momentum operator, and $\hat{\mathbf{s}}$ is the spin operator. The whole Hamiltonian can be expressed as $\widehat{H} = \widehat{H}_0 + \widehat{H}_{soc}$, where $\widehat{H}_0$ is the TB Hamiltonian for spinless particles and $\widehat{H}_{soc}$ is the SOC part. Explicitly, we can express the SOC Hamiltonian in the spin orbital basis as

$$\begin{aligned}\widehat{H}_{soc} &= \sum_{Ri\alpha\beta,s,s'} \underbrace{\langle\varphi_{Ri\alpha s}|\lambda_i\hat{\boldsymbol{L}}\cdot\hat{\mathbf{s}}|\varphi_{Ri\beta s'}\rangle}_{\zeta_{Ri\alpha s,R'j\beta s'}} \hat{a}^{\dagger}_{i\alpha s}(R)\hat{a}_{i\beta s'}(R)\\ &= \sum_{Ri\alpha\beta,s,s'} \zeta_{i\alpha s,i\beta s'}\hat{a}^{\dagger}_{i\alpha s}(R)\hat{a}_{i\beta s'}(R),\end{aligned}$$

where the indices are same to those in $\widehat{H}_0$ except that s, s' represent the spin degree of freedom (up or down along the quantization axis).

So far, we deal with the system without magnetic order, while sometimes magnetism is ubiquitous. In order to generalize the TB approach to magnetic materials, we take mean field approximation to deal with the many-body interaction with an exchange field.[34–36] In this case, we can write the Hamiltonian as $\widehat{H} = \widehat{H}_0 + \widehat{H}_{ex}$. The exchange field term can be expressed as $\widehat{H}_{ex} = -\sum_i J_i^{ex}\boldsymbol{m}_i\cdot\hat{\boldsymbol{s}}$, where J_i^{ex} is the effective exchange field strength of the ith atom and $\boldsymbol{m}_i$ is the unit direction vector of magnetic momentum of the ith atom. Here, $\hat{\boldsymbol{s}}$ is the electron spin operator. In the second quantization notation, the Hamiltonian of the exchange field can be written as

$$\begin{aligned}\widehat{H}_{ex} &= -\sum_{Ri\alpha s,R'j\beta s'} \underbrace{\varphi_{Ri\alpha s}|J_i^{ex}\hat{\boldsymbol{m}}_i\cdot\hat{\boldsymbol{s}}|\varphi_{R'j\beta s'}}_{\mathcal{B}_{Ri\alpha s}}\hat{a}^{\dagger}_{i\alpha s}(R)\hat{a}_{j\beta s'}(R')\\ &= -\sum_{Ri\alpha s}\mathcal{B}_{Ri\alpha s}\hat{a}^{\dagger}_{i\alpha s}(R)\hat{a}_{i\alpha s}(R),\end{aligned}$$

where the basis functions are orthogonal to each other. Note that for some magnetic order, one may need to adopt a magnetic unit cell larger than the chemical unit cell to accommodate the large period of the magnetic order. The total TB Hamiltonian of the magnetic materials can be written as $\widehat{H} = \widehat{H}_0 + \widehat{H}_{soc} + \widehat{H}_{ex}$.

With the TB method implemented in the PASP package, one can gain insight into the physical phenomena related to the electronic structures. For instance, we investigated the microscopic mechanism of ferroelectricity in 2D SnTe,[37] revealed the origin of Kitaev interactions in 2D magnets,[38] and reconciled the contradiction between experiment and previous theory on the multiferroicity in triangular lattice magnets.[39]

2. Effective magnetic Hamiltonian

Here, we discuss the effective magnetic Hamiltonian. For a magnetic system with localized moments, the exchange interactions between the magnetic ions are usually of the symmetric Heisenberg-type. In some cases (e.g., large SOC systems), we need to consider other interactions such as antisymmetric Dzyaloshinskii–Moriya (DM) exchange, anisotropic symmetric exchange, and single-ion magnetic anisotropy (SIA). We can combine all these bilinear interactions to express this Hamiltonian in a succinct matrix form as $H_{spin} = \sum_{i,j}\vec{S}_i\cdot\widehat{J_{ij}}\cdot\vec{S}_j + \sum_{ii}\vec{S}_i\cdot\widehat{A_{ii}}\cdot\vec{S}_i + \ldots$, where the 3×3 matrices $\widehat{J_{i,j}}$ and $\widehat{A_{ii}}$ describe exchange interactions and single-ion magnetic anisotropy, respectively. In general, the single-ion magnetic anisotropy term has the general form as $H_{SIA} = A_{xx}S_x^2 + A_{yy}S_y^2 + A_{zz}S_z^2 + 2A_{xy}S_xS_y + 2A_{xz}S_xS_z + 2A_{yz}S_yS_z$. When the ion has easy-axis or easy-plane anisotropy with the direction or normal along the z axis, the SIA Hamiltonian can be simplified to $H_{SIA} = A_{zz}S_z^2$.

The parameters of the spin Hamiltonian can be obtained by performing first-principles calculations. We first find out the symmetrically inequivalent magnetic pairs within a given cutoff distance. To evaluate the interacting parameters of a given magnetic pair in an accurate and easy way, we developed the so-called "four-state method" in which the energies of four specially designated spin states of a supercell are computed with a first-principles method.[40] For example, we can evaluate the isotropic Heisenberg interaction J by calculating the total energies of the following four states of ↑↑, ↑↓, ↓↑, and ↓↓, whose energies are E_1, E_2, E_3, and E_4, respectively. Here, the arrows represent the directions of two magnetic ions of the interaction pair, while other magnetic ions adopt the same low-energy spin state. The Heisenberg exchange interaction parameter can be computed as $J = (E_1 - E_2 - E_3 + E_4)/4S^2$, where S is the spin value of the magnetic ion. Similarly, this method can also be adopted to determine the parameters of DM interactions, Kitaev interactions, and single-ion magnetic anisotropy.[16,20–23,38,40–57] For iterant metallic systems, the high-order spin Hamiltonian beyond the second-order bilinear Hamiltonian may be necessary for describing the magnetic behavior. In these cases, we will resort to the

machine learning method for estimating the parameters of a complex Hamiltonian in the following discussion.

3. Effective Hamiltonian for ferroelectrics

Here, we introduce the effective Hamiltonian for ferroelectrics. As the ferroelectric structure can be viewed as a superimposition of small atomic distortions to the high symmetry paraelectric structure, we select local atomic displacement modes and strain as degrees of freedom for describing the ferroelectric state. Following Vanderbilt and his co-workers,[58,59] the effective Hamiltonian for ferroelectrics in our package contains five parts including the local-mode self-energy (E^{self}), the long-range dipole–dipole interaction (E^{dpl}), the short-range interaction between soft modes (E^{short}), the elastic energy (E^{elas}), and the interaction between the local modes and local strain (E^{int}),

$$H_{FE} = E^{\text{self}}(\{\boldsymbol{u}\}) + E^{\text{dpl}}(\{\boldsymbol{u}\}) + E^{\text{short}}(\{\boldsymbol{u}\}) + E^{\text{elas}}(\{\eta_l\}) + E^{\text{int}}(\{\boldsymbol{u}\},\{\eta_l\}),$$

where $\boldsymbol{u}$ represents the amplitude vector of the local soft mode and η_l is the local strain tensor in the Voigt notation. The self-energy part can be written as $E^{\text{self}}(\{\boldsymbol{u}\}) = \sum_i \text{E(ui)}$, where $E(\boldsymbol{u_i})$ is the energy of an isolated local mode at cell $\boldsymbol{R_i}$ with amplitude $\boldsymbol{u_i}$, relative to that of the paraelectric structure. By Taylor expansion, $E(\boldsymbol{u_i})$ usually includes all the symmetrically allowed terms up to fourth order because the anharmonic contributions are important to self-energy. As for the dipole–dipole interaction $E^{\text{dpl}}(\{\boldsymbol{u}\})$ and the short-range interaction $E^{\text{short}}(\{\boldsymbol{u}\})$, we can combine them by adopting the second-order pair interaction $E^{\text{pair}}(\{\boldsymbol{u}\}) = \frac{1}{2}\sum_{i\neq j}\sum_{\alpha\beta} J_{ij,\alpha\beta} u_{i\alpha} u_{j\beta}$. The elastic energy $E^{\text{elas}}(\{\eta_l\})$ is evaluated with the elastic constants of the paraelectric structure. To describe the coupling between strain and local modes, we can consider the dependence of the second-order on-site interaction on the strain, namely, $E^{\text{int}}(\{\boldsymbol{u}\},\{\eta_l\}) = \frac{1}{2}\sum_i \sum_{l\alpha\beta} B_{l\alpha\beta}\eta_l u_\alpha(\boldsymbol{R_i}) u_\beta(\boldsymbol{R_i})$.[58] Note that our package could also include higher order terms for $E^{\text{short}}(\{\boldsymbol{u}\})$ and $E^{\text{int}}(\{\boldsymbol{u}\},\{\eta_l\})$ if necessary.

Knowing the general form of the effective Hamiltonian for ferroelectrics, we can generate a set of distorted structures and calculate their total energies with the first-principles method to fit the undetermined parameters. For ferroelectrics with a complex effective Hamiltonian containing hundreds of possible parameters, we can also adopt the machine learning method, which will be discussed in the following paragraphs. After constructing the effective Hamiltonian, we can investigate the thermodynamic and kinetic properties of ferroelectric materials by performing Monte Carlo simulations and molecular dynamics simulations. For example, we apply our method to treat the 2D ferroelectric material SnTe.[37] By performing Monte Carlo simulations with the effective Hamiltonian, we find that the Curie temperature of a defect-free thin film could be higher than that of a perfect bulk system, in agreement with the experimental findings.[60]

4. Effective Hamiltonian for multiferroics

Multiferroics form a class of materials that can show simultaneously ferroelectric and magnetic ordering, which provide an ideal platform for electric field control of magnetism due to the intrinsic magnetoelectric couplings.[61] To describe the interplay between different degrees of freedom in multiferroics, in general, the effective Hamiltonian H_{mul} should consist of three parts: magnetic effective Hamiltonian H_{spin}, effective Hamiltonian for ferroelectrics H_{FE}, and spin-lattice coupling term $H_{coupling}$. The coupling term $H_{coupling}$ describes the couplings between spin and structural modes (including the local soft mode, strain, and anti-ferroelectric degrees of freedom).

The unified polarization model is implemented in PASP to compute the spin-order-induced polarization.[39,51,55,57,62,63] In our model, the total polarization can be written as a sum of two parts, that is, $\mathrm{P} = \mathbf{P_e}(\mathbf{S};\ \mathbf{U} = 0,\ \eta = 0) + \mathbf{P_{lat}}(\mathrm{U},\ \eta)$, where $\mathbf{P_e}$ is the electronic contribution induced by the spin order $\mathbf{S}$ and $\mathbf{P_{lat}}$ is the lattice contribution due to the ionic displacements $\mathbf{U}$ and strain η. Due to time-reversal symmetry, $\mathbf{P_e} = \sum_{i,\alpha\beta} P^i_{\alpha\beta} S_{i\alpha} S_{i\beta} + \sum_{\langle i,j\rangle,\alpha\beta} P^{ij}_{\alpha\beta} S_{i\alpha} S_{i\beta}$, where the first term is the single-site term, while the second term is the inter-site term. The inter-site term includes the general spin current contribution, the symmetric exchange striction contribution, and the anisotropic symmetric exchange contribution. To obtain $\mathbf{P_{lat}}$, the total effective Hamiltonian $\mathrm{H}(\mathbf{S};\ \mathbf{U},\ \eta)$ should be minimized with respect to the ionic displacements $\mathbf{U}$ and strain η for a given fixed spin order $\mathbf{S}$. These interacting parameters in the unified model can be computed with our four-state method.[40] With this unified polarization model, we demonstrate that our model not only correctly describes the ferroelectricity in MnI_2 but also overcomes the limitation of the previous existing models.[39]

5. Machine learning method for constructing realistic effective Hamiltonian

The traditional way to obtain an effective Hamiltonian is by proposing a form with several undetermined parameters and then performing the linear least squares to fit first-principles results. However, sometimes it can be difficult to determine an appropriate effective Hamiltonian with all important interactions but without redundant ones. For example, in metallic and narrow gap magnets, the many-body and high-order interactions may be important to describe the magnetic properties so that there are too many possible interacting terms to be treated by the traditional way.[64]

To deal with these fitting difficulties, we develop a general and efficient machine learning (ML) approach.[65] Our ML algorithms not only help avoid over-fitting problems but also significantly improve the efficiency of the searching for major interaction terms. In our method, we first derive the effective Hamiltonian considering all the possible interaction terms. Then, we use our ML algorithm accompanied with multiple linear regression analyses to extract the important terms and construct the effective Hamiltonian. We can reserve those important terms and discard the negligible ones. In this way, our effective Hamiltonian will possess a succinct form and deliver a clear physical picture.

For practical cases, effective Hamiltonians can be described as the linear combinations of some basis functions as $H_{\text{eff}} = \sum_{j=1}^{p_{max}} C_j h_j$, where $\{h_j\}$ is the set of basis functions and $\{C_j\}$ is their undetermined coefficients. In general, it is necessary to perform truncations in expansion order and interaction distances, which can restrict

the terms of $\{C_j h_j\}$. The forms and the number of the basis functions can be different according to the specific physical system. After the simplifications by truncations and symmetry analyses, the number of interaction terms can be greatly decreased, but it may be still too large to be identified by traditional linear least squares fittings.

In our package, we use the ML algorithm accompanied with multiple linear regression analyses to extract the important terms out of the p_{max} possible terms. Supposing that p terms are selected, we can renumber the subscripts (j's) and use $\{b_j\}_{j=1}^{p}$ to denote the coefficients $\{C_j\}$ so that the effective Hamiltonian can be written as $H_{\text{eff}} = \sum_{j=1}^{p} b_j h_j$. The value of b_j given by multiple linear regression analyses is denoted by $\widehat{b_j}$. The variance of the difference between the predicted value $\widehat{H}_{\text{eff}}^{(i)} = \sum_{j=1}^{p} \widehat{b_j} h_j$ ($i = 1, \ldots, n$) and the actual value $H_{\text{eff}}^{(i)}$ (given by *ab initio* calculations or experimental data) is denoted by σ^2, which can be estimated either by the training set, validation set, or testing set, with the estimated value denoted by $\widehat{\sigma^2}$, $\widehat{\sigma'^2}$, or $\widehat{\sigma_v^2}$, respectively. We use $(\sigma^2 \cdot \lambda^p)$ ($\lambda \geq 1$) as the criterion for selecting better models, where λ^p is a penalty factor in favor of the models with less parameters. To search for the best model (which has the least value of $\sigma^2 \cdot \lambda^p$), we can start from $p = 1$ (the constant term) as $H_{\text{eff}} = b_1 h_1$, with $h_1 \equiv 1$. We can also start from any set of initial p parameters. Then, we can try adding, deleting, or substituting a term $(b_j h_j)$ into or from our temporary model to see whether the model has better performance. If so, we accept the new model and continue trying adding, deleting, or substituting a term until no better model can be found. In practice, when we finish the search with a certain value of λ, we can repeat the searching with other λ. Finally, we can select one model among these best models (corresponding to different λ values) according to their predicting performance on the testing set ($\widehat{\sigma'^2}$). Our benchmarks show that our method performs better than the traditional method of constructing effective Hamiltonians, not only in efficiency but also in reliability.[65]

Our ML approach is generally applicable to various physical systems with different effective Hamiltonians. For example, we apply our ML approach to study the magnetic interactions in the multiferroic material $TbMnO_3$.[65] Our approach not only reproduces the known results that the Heisenberg, biquadratic, and ring exchange interactions are the major magnetic interactions[64] but also finds out that the next most important magnetic interactions are three three-body fourth-order interactions with different spatial configurations.

6. Effective Hamiltonian in terms of machine learning potential

Machine learning has become one of the most important computational tools in condensed matter physics.[66–68] In particular, the artificial neural network (ANN) can link the correlation between features and target labels with no explicit mathematical expressions. After training, we can use ANN to predict the labels with features, which is an ideal method for exploring hidden relationship between physical properties.

In our package, we use ANN instead of the polynomial form to fit the potential-energy surface with the data obtained from the first-principles calculations. Our package can load ANN from the open source library PyTorch.[69] Several kinds of ANN are available with high accuracy. The classic ANN, i.e., multilayer fully connected layers, accompanied with the Batch Normalization (BN) method[70] have been implemented in our package. To get training data, we can generate random configurations and use first-principles calculations to calculate their total energies. We note that we need to transform the configurations into appropriate descriptors, which will improve the efficiency and accuracy of ANN. When training the neural network, descriptors are propagated forward through the neural network, while the total energies are used as the output data. After training a certain number of epochs, the parameters of the neural network become stable and we can use the testing data to check the accuracy of the neutral network. Our machine learning-based effective Hamiltonian method can be adopted to investigate complicated materials that are hard to be described by the usual effective Hamiltonian method based on polynomial potentials.

D. Monte Carlo simulation

The Monte Carlo (MC) simulation with an effective Hamiltonian is widely adopted to investigate the ground state at zero temperature and simulate the temperature-dependent phase transition. In a condensed matter system, there may exist a huge number of local minima in the energy surface. However, with the decrease in temperature, the configuration may be trapped in one of the local minima separated by high energy barriers. In this case, the characteristic time of getting out of a local minimum will increase rapidly. This problem will greatly limit the efficiency and reliability of usual Metropolis Monte Carlo simulations. Therefore, several methods were proposed to overcome this problem, and one reliable way is to perform a simulation with a generalized ensemble (such as the multi-canonical algorithm[71] and simulated tempering[72]).

In our package, we implement not only the usual Metropolis MC algorithm but also the parallel tempering algorithm, which can be regarded as a parallelized version of the simulated tempering but with different extended ensemble.[73,74] The flowchart of our parallel tempering Monte Carlo (PTMC) method is shown in Fig. 3. In the usual Metropolis MC simulation, the state is characterized by a set of generalized coordinates. However, in PTMC simulation, we can consider the physical system consisting of M replicas $\{X\} = \{X_1, X_2, \cdots, X_M\}$ at M temperatures $\{T\} = \{T_1, T_2, \cdots, T_M\}$, respectively. Each replica (e.g., the mth replica) can be described by a common Hamiltonian $H(X_m)$ associated with inverse temperature β_m, where $\beta_m = \frac{1}{k_B T_m}$, where k_B is the Boltzmann constant. For convenience, we assume that $\beta_m < \beta_{m+1}$. Note that each replica is in contact with its own heat bath and has no interaction with other replicas. In this case, the partition function can be written as $\Xi = \text{Tr}_{\{X\}} \exp\left(-\sum_{m=1}^{M} \beta_m H(X_m)\right) = \prod_{m=1}^{M} Z(\beta_m)$, where $Z(\beta_m)$ is the partition function for the mth replica. For a specific temperature $\{\beta\}$, the probability of finding $\{X\}$ is $P(\{X, \beta\}) = \prod_m^M Z^{-1}(\beta_m) \exp[-\beta H(X_m)]$. When performing the MC simulation, one should construct a Markov process to reach the equilibrium distribution by introducing the transition matrix $W(X, \beta_m | X', \beta_n)$, i.e., the probability of exchanging configurations between the nth and mth replicas. In order to make sure that

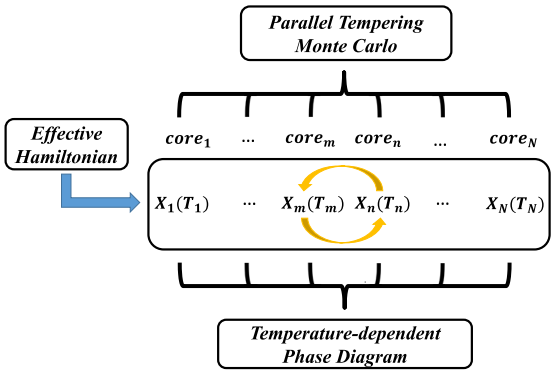

FIG. 3. The flowchart of parallel tempering Monte Carlo simulation. The number of replicas should be equal to or divided by the number of CPU cores. Each replica is simulated simultaneously and independently by the canonical Metropolis MC method with the effective Hamiltonian. Exchange of two configurations X_m and X_n is tried by referring to the energy cost with the probability of $W(X_m, \beta_m | X_n, \beta_n)$. After all replicas reach the equilibrium distribution, one can perform measurements to obtain the temperature-dependent phase diagram.

each replica converges to its equilibrium distribution, the transition matrix should satisfy $W(X, \beta_m | X', \beta_n) / W(X', \beta_m | X, \beta_n) = \exp(-\Delta)$, where $\Delta = (\beta_n - \beta_m)[H(X) - H(X')]$. When we adopt the Metropolis method, the transition probability of the replica-exchange part can be expressed as $W(X, \beta_m | X', \beta_n) = \min(1, \exp(-\Delta))$.

In practice, we perform the PTMC simulations with the following two steps alternately: (i) Each replica is simulated simultaneously and independently as canonical ensemble with standard MC method. (ii) Exchange of two configurations X_m and X_{m+1} is tried by computing the probability of $W(X_m, \beta_m | X_{m+1}, \beta_{m+1})$ with the energy difference. Here, we restrict the replica-exchange process to neighboring temperatures since the acceptance ratio of the replica-exchange decreases exponentially with the difference $\beta_m - \beta_{m+1}$. In this way, the simulations can easily escape from the local minimum and greatly reduce relaxation time to reach the thermal equilibrium quickly.

Another important question is about the temperature mesh. We should give a suitable temperature mesh since more replicas at low temperature will give a more reliable result about the ground state but with more computational cost. Of course, we should also sample high temperature replicas to simulate the temperature-dependent phase transition. In our package, we have two different temperature meshes. In the first choice, the temperature T is evenly distributed according to 1/T, while in the second one, the temperature T is evenly distributed according to T. The user can also set the temperature mesh manually. We have also implemented several other techniques to improve the MC performance. First, we can adopt the heat bath algorithm[75] to accelerate MC simulations whenever possible. Second, after the MC simulations, the conjugate gradients (CG) method[76] can be applied to further optimize the configuration and reach the energy local minima. Our PTMC method is so general that it can be adopted to predict the ground state and phase transition of different kinds of physical systems.[16,20–23,37,38,40–57]

We note that we have integrated the symmetry analysis, effective Hamiltonian method, and PTMC simulation in a single package. That is to say, our package can automatically give the general form of an effective Hamiltonian according to the symmetry analyses. Then, our package can generate some configurations with different supercells and automatically submit the first-principles calculation jobs to obtain their corresponding total energies. After that, our package can use the machine learning approach to construct a realistic effective Hamiltonian using these total energies (and forces in the case of ferroelectrics). With the effective Hamiltonian, our package can perform PTMC simulation to predict the ground state and thermodynamic properties.

III. USAGE AND EXAMPLES

In this section, we discuss the installation of our package and the main input files. Then, we take $BiFeO_3$ as an example to demonstrate the power of our GA global structure searching method. After that, we take Zn_2FeOsO_6 as an example to show the PTMC method.

A. Installation

Our PASP package is mainly written with Fortran 90, except that some machine learning methods are coded using python. To install PASP, one need a MPI-enabled Fortran 90 compiler (e.g., Intel Fortran compiler) since our package can run in parallel. In addition, one need BLAS, FFTW, and LAPACK libraries. When compile PASP, one needs to modify *src/arc.make* according to the compiling environment. We note that the *arch.make* can determine the way that *Makefile* generate the executable file, and one do not need to edit the *Makefile*. Once we configure the compiling environment, we can enter "make" to obtain the executable binary file.

B. Main input files

The main input file "lattice_model.fdf" with the FDF format contains the main parameters for the simulation. The FDF format allows data to be given in any order or to be omitted with default values. All text following the character "#" is taken as comment. The FDF syntax is a "data tag" followed by its value. Values can be assigned by the default value. Logical values can be given as T (True) or F (False). Some complex data are treated as blocks and are placed between "%block label" and "%endblock label" ("label" can be different, e.g., Z_values). If the same tag is specified more than once, only the first one will be used. The tag "Model" in lattice_model.fdf indicates the function feature of the simulation.

C. Example 1: Global structure prediction

In this section, we take $BiFeO_3$ as an example to perform GA global structure searching.

1. Input files

The following variables are included in lattice_model.fdf:

```
Model GA
%include str.ANI
%block Z_values
83 26 8
%endblock Z_values
GA.population_size 30
GA.max_generation 20
save_str.nsave_str 10
GA.magnetic T
%block Spin_values
0 5 0
%endblock Spin_values
GA.random_magnetic F
GA.lread_OUTCAR_mag F
GA.perturbation T
GA.Pher 0.75
GA.Pmut 0.25
GA.gen_ran_str_sym F
GA.spg_front 1
GA.spg_rear 230
GA.fix_cell F
```

Here follows a description of these variables discussed above, including the data types.

Another input file is str.ANI, which is originated from POSCAR and contains the atomic positions under the Cartesian format. In our PGA method, we need a high symmetry state to generate distorted child structure. Here, the cubic configuration is adopted to show the str.ANI.

Here follows a description of these variables discussed above.

```
NumberOfAtoms 20
number_of_species 3
LatticeConstant 1 Ang
%block LatticeVectors
5.5225 0.0 0.0
0.0 5.5225 0.0
0.0 0.0 7.81
%endblock LatticeVectors
AtomicCoordinatesFormat NotScaledCartesianAng
%block AtomicCoordinatesAndAtomicSpecies
2.761250000000 0.000000000000 0.000000000000 1 Bi 1
2.761250000000 0.000000000000 3.905000000000 1 Bi 2
. . .
. . .
1.380625000000 1.380625000000 1.952500000000 3 O 20
%endblock AtomicCoordinatesAndAtomicSpecies
```

NumberOfAtoms: the total number of atoms in the system.
number_of_species: the number of different elements in the system.
LatticeConstant: the unit of length in the system.
%block LatticeVectors: the lattice parameters of the system.
%block AtomicCoordinatesAndAtomicSpecies: the atomic coordinates under the cartesian format. Note that the serial number of element, the symbol of element, and the serial number of atom are appended to the corresponding atom.

2. Output files

The most important output files of GA global structure searching simulations are the low-energy structures named as Saved_*.POS. They are arranged by the total energy from low to

Model: the function feature of the simulation.
%include str.ANI: the file of str.ANI is required to perform GA simulations.
%block Z_values and %endblock Z_values (integer): the atomic number of each elements.
GA.population_size: the population size.
GA.max_generation: the maximum number of GA iterations.
save_str.nsave_str: the number of low-energy structures saved during the simulations.
GA.magnetic: if True, the magnetic degree is included in the GA simulations.
%block Spin_values and %endblock Spin_values: the local magnetic moment of each elements.
GA.random_magnetic: if True, the magnetic configuration is generated completely randomly.
GA.lread_OUTCAR_mag: if True, the magnitude of local magnetic moment is optimized during the GA simulations by reading the optimized local moments from OUTCAR and replacing the old values.
GA.perturbation: if True, the PGA method is adopted to evolve the structures.
GA.Pher: the probability of heredity to generate child structures.
GA.Pmut: the probability of mutation to generate child structures.
GA.gen_ran_str_sym: if True, the initial random structures are generated by the symmetry of space groups ranging from "GA.spg_front" to "GA.spg_rear."
GA.spg_front: the front of the space group that is adopted to generate initial random structures.
GA.spg_rear: the rear of the space group that is adopted to generate initial random structures.
GA.fix_cell: if True, the lattice are fixed during the optimization of the structures.

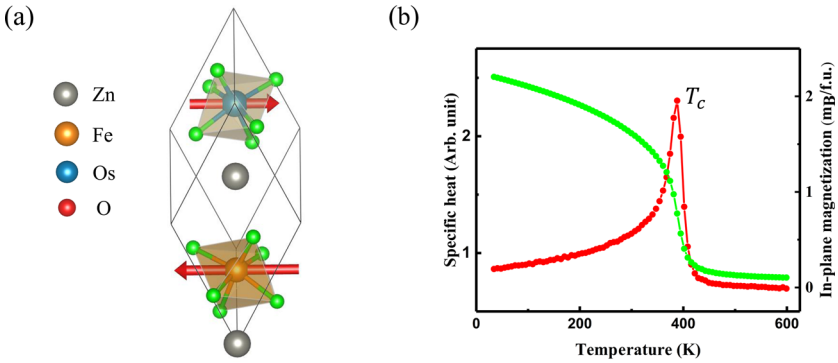

FIG. 4. The application of parallel tempering Monte Carlo simulation. (a) The ground state of Zn_2FeOsO_6 predicted by GA global structure searching. Our Monte Carlo simulation reproduces its magnetic ground state with Curie temperature (T_c) of 394 K. (b) The specific heat and the total spin moment (M_{ab}) as a function of temperature.

high. They have the format of POSCAR, and the space group ID is also attached at the end of Saved_*.POS. When we consider the magnetic degree, the magnetic configuration is also appended at the end of files.

3. Results

Generally speaking, the PGA method can reduce the searching space, and it is much more efficient than the FGA method. In $BiFeO_3$, we search not only the atomic configuration but also the magnetic state. Here, we do not consider the SOC effect. The evolution of total energies during our PGA iterations is shown in Fig. 2(c). The number of generations is set to be 20, and each generation includes a population of 30 individual structures. As a comparison, the normal FGA (i.e., generate the initial structure with the random-selected space group and generate the child structure by the normal cut-and-splice operation) simulations are performed with same calculation parameters [see Fig. 2(d)]. In PGA simulations, we find the ground structural and magnetic configuration on the fourth generation. For comparison, the FGA simulations take 11 generations to identify the ground state. The trend of average energy at each generation also demonstrates the high efficiency of PGA simulations. We repeat each simulation several times to check the reliability of our results. Our PGA simulations successfully find the correct ground state within five generations, while the FGA simulations will cost much more computational resource. Therefore, this benchmark suggests that our newly developed GA methods are powerful in predicting not only the crystal structures but also the magnetic configurations.

```
Model Spin_lattice_interaction
%include str.ANI
MC T
nblk 500
nbeg_blk 2000
Parallel_Tempering T
PT.M 96
VPT.low_temp 0.0001
PT.high_temp 0.002
PT.niter 1
PT.nblk_T 4000
PT.Tmesh 1
%block SuperCell
8 0 0
0 8 0
0 0 8
%endblock SuperCell
%block Z_values
30 26 76 8
%endblock Z_values
%block isaAB
2 3
%endblock isaAB
%block Spin_values
0 5 3 0
%endblock Spin_values
global.heat_bath F
```

D. Example 2: Parallel tempering Monte Carlo simulation

In this section, we take Zn_2FeOsO_6 as an example to perform PTMC simulations. Our GA global structure searching shows that

Model (string): the function feature of the simulation.
%include str.ANI: the file of str.ANI is required to perform MC simulations.
MC: if True, we perform MC simulations.
Parallel_Tempering: if True, we perform parallel tempering MC (PTMC) simulations.
PT.M: number of replicas.
PT.low_temp: the lowest temperature (Hartree) of MC simulations.
PT.high_temp: the highest temperature (Hartree) of MC simulations.
PT.niter: number of PT iteration.
PT.nblk_T: number of exchange steps.
PT.Tmesh: temperature mesh. 1: evenly distributed according to 1/T; 2: evenly distributed according to T.
%block SuperCell: the supercell of the structure specified in str.ANI.
%block isaAB: the interactions between different magnetic ions.
%block Z_values and %endblock Z_values (integer): the atomic number of each elements.
global.heat_bath: if True, use heat bath method instead of standard Metropolis method.

```
4 # units in eV and Ang
1.5022     −2.6020     4.5948
1.5022      2.6020     4.5948
−3.0045     0.0000     4.5948
1           0.0317     2     3     0.0000     0.0000     3.0345     3.0045     0.0000     5.2654
2           0.0296     2     3     0.0000     0.0000     3.0345     1.5022     2.6020     0.6705
3           0.0073     3     3     0.0000     0.0000     9.8603    −0.0000     5.2041     9.8603
4           0.0032     3     3     0.0000     0.0000     9.8603     1.5022     2.6020    14.4552
```

Zn_2FeOsO_6 has a ferrimagnetic ground state with a polar space group $R3$ [see Fig. 4(a)].[20] In our PTMC simulations, we need an effective Hamiltonian model to calculate the total energies. Here, we adopt the spin Hamiltonian discussed in our previous work.[20]

1. Input files

The following variables are included in lattice_model.fdf:

Here follows a description of these variables discussed above, including the data types.

Another input file of spin_exchange.dat defines the interactions between magnetic ions.

The first line denotes the number of interactions, followed by the lattice parameters of the unit cell. In line 4, the first number "1" denotes the first interaction, followed by the J value (in the unit of eV). "2" and "3" denote the interaction between Fe and Os (Fe is the second type ion and Os is the third type ion in str.ANI). After that, we attach the coordinates of Fe and Os. Here, we adopt the general Heisenberg model $H_{spin} = \sum J_{ij}\vec{S}_i \cdot \vec{S}_j$. In Zn_2FeOsO_6, it has strong antiferromagnetic interaction between Fe and Os ions with $J_1 = 31.7$ meV and $J_2 = 29.6$ meV. Here, the spin interaction parameters are effective by setting the spin value of Fe and Os to 1 μB. The antiferromagnetic interactions between Os ions are much weaker with $J_3 = 7.3$ meV and $J_4 = 3.2$ meV.

2. Output files

The most important output files from the MC simulation are *C_PTMC.dat* and *M_PTMC.dat*, which show the temperature-dependent variation of heat capacity and magnetism, respectively. Another output file *lowest_onlyspin.xsf* shows the magnetic ground state.

3. Results

Using the magnetic effective Hamiltonian discussed in our previous paper,[20] we obtain the thermodynamic behavior of the magnetism and identify its ferrimagnetic ground state (see Fig. 4). The peak in the specific heat curve indicates that the ferrimagnetic Curie temperature (T_C) is about 394 K. In conclusion, our PTMC simulations reproduce the correct magnetic ground state and suggest that Zn_2FeOsO_6 is a room temperature multiferroic material.

IV. SUMMARY

We introduce a powerful software package called PASP (Property Analysis and Simulation Package for materials), which implements several functional features including symmetry analysis, global structure searching, effective Hamiltonian methods, and Monte Carlo simulation. We discussed methodologies of these functional features. PASP has been widely used to treat condensed matter physical systems, which not only demonstrate the reliability of our package but also encourage further developments. In principle, PASP is compatible with any first-principles codes. Currently, PASP implemented the interface with Vienna *ab initio* Simulation Package (VASP).[77,78] In the future, we plan to implement interfaces with other first-principles codes. Furthermore, we will add some new functionalities to PASP. For example, we will implement molecular dynamics and spin dynamics for studying the dynamic behavior of ions and spins in complex condensed matter systems. In addition, we will incorporate the electron's orbital and charge degrees of freedom into the effective Hamiltonian for investigating exotic phenomena such as orbital-ordering and/or charge-ordering. We hope that our package will be adopted by more researchers working in computational material science and computational physics to solve cutting edge science problems.

ACKNOWLEDGMENTS

This work was supported by the NSFC (Grant Nos. 11825403 and 11991061), the Program for Professor of Special Appointment (Eastern Scholar), and the Qing Nian Ba Jian Program. J.S.F. acknowledges support from the Anhui Provincial Natural Science Foundation (Grant No. 1908085MA10) and the Opening Foundation of State Key Laboratory of Surface Physics Fudan University (KF2019_07). We thank Dr. W. Luo, Dr. K. Liu, Dr. Z. J. Jiang, Dr. C. S. Xu, and Mr. J. Y. Ni for useful discussions.

DATA AVAILABILITY

The data that support the findings of this study are available from the corresponding author upon reasonable request.

REFERENCES

[1] Y. Wang, J. Lv, L. Zhu, and Y. Ma, "CALYPSO: A method for crystal structure prediction," Comput. Phys. Commun. **183**, 2063–2070 (2012).
[2] C. W. Glass, A. R. Oganov, and N. Hansen, "USPEX: Evolutionary crystal structure prediction," Comput. Phys. Commun. **175**, 713–720 (2006).
[3] A. van de Walle, M. Asta, and G. Ceder, "The alloy theoretic automated toolkit: A user guide," Galphad **26**, 539–553 (2002).
[4] M. S. Dresselhaus, G. Dresselhaus, and A. Jorio, *Group Theory: Application to the Physics of Condensed Matter* (Springer-Verlag, 2008).
[5] L. Fu and C. L. Kane, "Topological insulators with inversion symmetry," Phys. Rev. B **76**, 045302 (2007).

[6]K. Liu, W. Luo, J. Ji, P. Barone, S. Picozzi, and H. Xiang, "Band splitting with vanishing spin polarizations in noncentrosymmetric crystals," Nat. Commun. **10**, 5144 (2019).
[7]W. Luo, J. Ji, J. Lu, X. Zhang, and H. Xiang, "Two-dimensional topological semimetals protected by symmorphic symmetries," Phys. Rev. B **101**, 195111 (2020).
[8]C. J. Pickard and R. J. Needs, "*Ab initio* random structure searching," J. Phys.: Condens. Matter **23**, 053201 (2011).
[9]Y.-Y. Zhang, W. Gao, S. Chen, H. Xiang, and X.-G. Gong, "Inverse design of materials by multi-objective differential evolution," Comput. Mater. Sci. **98**, 51–55 (2015).
[10]A. R. Oganov and C. W. Glass, "Crystal structure prediction using *ab initio* evolutionary techniques: Principles and applications," J. Chem. Phys. **124**, 244704 (2006).
[11]T. Gu, W. Luo, and H. Xiang, "Prediction of two-dimensional materials by the global optimization approach," Wiley Interdiscip. Rev.: Comput. Mol. Sci. **7**, e1295 (2017).
[12]X. Luo, J. Yang, H. Liu, X. Wu, Y. Wang, Y. Ma, S.-H. Wei, X. Gong, and H. Xiang, "Predicting two-dimensional boron-carbon compounds by the global optimization method," J. Am. Chem. Soc. **133**, 16285–16290 (2011).
[13]D. J. Wales and J. P. K. Doye, "Global optimization by basin-hopping and the lowest energy structures of Lennard-Jones clusters containing up to 110 atoms," J. Phys. Chem. A **101**, 5111–5116 (1997).
[14]H. Xiang, S.-H. Wei, and X. Gong, "Structures of $[Ag_7(SR)_4]^-$ and $[Ag_7(DMSA)_4]^-$," J. Am. Chem. Soc. **132**, 7355–7360 (2010).
[15]H. J. Xiang, J. L. F. Da Silva, H. M. Branz, and S.-H. Wei, "Understanding the clean interface between covalent Si and ionic Al_2O_3," Phys. Rev. Lett. **103**, 116101 (2009).
[16]F. Lou, W. Luo, J. Feng, and H. Xiang, "Genetic algorithm prediction of pressure-induced multiferroicity in the perovskite $PbCoO_3$," Phys. Rev. B **99**, 205104 (2019).
[17]D. M. Deaven and K. M. Ho, "Molecular-geometry optimization with a genetic algorithm," Phys. Rev. Lett. **75**, 288–291 (1995).
[18]X.-Z. Lu and J. M. Rondinelli, "Epitaxial-strain-induced polar-to-nonpolar transitions in layered oxides," Nat. Mater. **15**, 951–955 (2016).
[19]X. Z. Lu, X. G. Gong, and H. J. Xiang, "Polarization enhancement in perovskite superlattices by oxygen octahedral tilts," Comput. Mater. Sci. **91**, 310–314 (2014).
[20]P. S. Wang, W. Ren, L. Bellaiche, and H. J. Xiang, "Predicting a ferrimagnetic phase of Zn_2FeOsO_6 with strong magnetoelectric coupling," Phys. Rev. Lett. **114**, 147204 (2015).
[21]J. W. Guo, P. S. Wang, Y. Yuan, Q. He, J. L. Lu, T. Z. Chen, S. Z. Yang, Y. J. Wang, R. Erni, M. D. Rossell, V. Gopalan, H. J. Xiang, Y. Tokura, and P. Yu, "Strain-induced ferroelectricity and spin-lattice coupling in $SrMnO_3$ thin films," Phys. Rev. B **97**, 235135 (2018).
[22]J. S. Feng, K. Xu, L. Bellaiche, and H. J. Xiang, "Designing switchable near room-temperature multiferroics via the discovery of a novel magnetoelectric coupling," New J. Phys. **20**, 053025 (2018).
[23]Y. S. Hou, H. J. Xiang, and X. G. Gong, "Intrinsic insulating ferromagnetism in manganese oxide thin films," Phys. Rev. B **89**, 064415 (2014).
[24]K. Xu, X.-Z. Lu, and H. Xiang, "Designing new ferroelectrics with a general strategy," npj Quantum Mater. **2**, 1 (2017).
[25]S. Konschuh, M. Gmitra, and J. Fabian, "Tight-binding theory of the spin-orbit coupling in graphene," Phys. Rev. B **82**, 245412 (2010).
[26]V. M. Pereira, A. H. Castro Neto, and N. M. R. Peres, "Tight-binding approach to uniaxial strain in graphene," Phys. Rev. B **80**, 045401 (2009).
[27]S. Reich, J. Maultzsch, C. Thomsen, and P. Ordejón, "Tight-binding description of graphene," Phys. Rev. B **66**, 035412 (2002).
[28]F. Zahid, L. Liu, Y. Zhu, J. Wang, and H. Guo, "A generic tight-binding model for monolayer, bilayer and bulk MoS_2," AIP Adv. **3**, 052111 (2013).
[29]E. Ridolfi, D. Le, T. S. Rahman, E. R. Mucciolo, and C. H. Lewenkopf, "A tight-binding model for MoS_2 monolayers," J. Phys.: Condens. Matter **27**, 365501 (2015).
[30]J. C. Slater and G. F. Koster, "Simplified LCAO method for the periodic potential problem," Phys. Rev. **94**, 1498 (1954).
[31]W. A. Harrison, *Electronic Structure and the Properties of Solids: The Physics of the Chemical Bond* (Courier Corporation, 1989).
[32]C. Kittle, *Introduction to Solid State Physics*, 7th ed. (Wiley India Pvt. Limited, 2007).
[33]W. Harrison, *Elementary Electronic Structure* (World Scientific Publishing Company, 1999).
[34]J. Masek, B. Velicky, and V. Janis, "A tight binding study of the electronic structure of MnTe," J. Phys. C: Solid State Phys. **20**, 59 (1987).
[35]S. Fang, R. K. Defo, S. N. Shirodkar, S. Lieu, G. A. Tritsaris, and E. Kaxiras, "*Ab initio* tight-binding Hamiltonian for transition metal dichalcogenides," Phys. Rev. B **92**, 205108 (2015).
[36]G. Allan, "Surface electronic structure of antiferromagnetic chromium," Surf. Sci. **74**, 79–88 (1978).
[37]K. Liu, J. Lu, S. Picozzi, L. Bellaiche, and H. Xiang, "Intrinsic origin of enhancement of ferroelectricity in SnTe ultrathin films," Phys. Rev. Lett. **121**, 027601 (2018).
[38]C. Xu, J. Feng, H. Xiang, and L. Bellaiche, "Interplay between Kitaev interaction and single ion anisotropy in ferromagnetic CrI_3 and $CrGeTe_3$ monolayers," npj Comput. Mater. **4**, 57 (2018).
[39]H. J. Xiang, E. J. Kan, Y. Zhang, M.-H. Whangbo, and X. G. Gong, "General theory for the ferroelectric polarization induced by spin-spiral order," Phys. Rev. Lett. **107**, 157202 (2011).
[40]H. Xiang, C. Lee, H.-J. Koo, X. Gong, and M.-H. Whangbo, "Magnetic properties and energy-mapping analysis," Dalton Trans. **42**, 823–853 (2013).
[41]H. J. Xiang, E. J. Kan, S.-H. Wei, M.-H. Whangbo, and X. G. Gong, "Predicting the spin-lattice order of frustrated systems from first principles," Phys. Rev. B **84**, 224429 (2011).
[42]J. H. Yang, Z. L. Li, X. Z. Lu, M.-H. Whangbo, S.-H. Wei, X. G. Gong, and H. J. Xiang, "Strong Dzyaloshinskii–Moriya interaction and origin of ferroelectricity in Cu_2OSeO_3," Phys. Rev. Lett. **109**, 107203 (2012).
[43]X. Z. Lu, M.-H. Whangbo, S. Dong, X. G. Gong, and H. J. Xiang, "Giant ferroelectric polarization of $CaMn_7O_{12}$ induced by a combined effect of Dzyaloshinskii–Moriya interaction and exchange striction," Phys. Rev. Lett. **108**, 187204 (2012).
[44]C. Xu, J. Feng, M. Kawamura, Y. Yamaji, Y. Nahas, S. Prokhorenko, Y. Qi, H. Xiang, and L. Bellaiche, "Possible Kitaev quantum spin liquid state in 2D materials with S = 3/2," Phys. Rev. Lett. **124**, 087205 (2020).
[45]C. Xu, J. Feng, S. Prokhorenko, Y. Nahas, H. Xiang, and L. Bellaiche, "Topological spin texture in Janus monolayers of the chromium trihalides $Cr(I,X)_3$," Phys. Rev. B **101**, 060404 (2020).
[46]J. Y. Ni, P. S. Wang, J. L. Lu, and H. J. Xiang, "Realizing magnetoelectric coupling with hydrogen intercalation," Phys. Rev. Lett. **122**, 117601 (2019).
[47]C. Xu, B. Xu, B. Dupe, and L. Bellaiche, "Magnetic interactions in $BiFeO_3$: A first-principles study," Phys. Rev. B **99**, 104420 (2019).
[48]B. Xu, B. Dupé, C. Xu, H. Xiang, and L. Bellaiche, "Revisiting spin cycloids in multiferroic $BiFeO_3$," Phys. Rev. B **98**, 184420 (2018).
[49]K. Xu, J. S. Feng, Z. P. Liu, and H. J. Xiang, "Origin of ferrimagnetism and ferroelectricity in room-temperature multiferroic ε-Fe_2O_3," Phys. Rev. Appl. **9**, 044011 (2018).
[50]Y. S. Hou, H. J. Xiang, and X. G. Gong, "Unveiling the origin of the basal-plane antiferromagnetism in the spin-orbit Mott insulator Ba_2IrO_4: A density functional and model Hamiltonian study," New J. Phys. **18**, 043007 (2016).
[51]P. S. Wang, X. Z. Lu, X. G. Gong, and H. J. Xiang, "Microscopic mechanism of spin-order induced improper ferroelectric polarization," Comput. Mater. Sci. **112**, 448–458 (2016).
[52]K. Liu, Y. Hou, X. Gong, and H. Xiang, "Orbital delocalization and enhancement of magnetic interactions in perovskite oxyhydrides," Sci. Rep. **6**, 19653 (2016).
[53]H.-F. Zhu, H.-Y. Cao, Y. Xie, Y.-S. Hou, S. Chen, H. Xiang, and X.-G. Gong, "Giant biquadratic interaction-induced magnetic anisotropy in the iron-based superconductor $A_xFe_{2-y}Se_2$," Phys. Rev. B **93**, 024511 (2016).
[54]Y. S. Hou, H. J. Xiang, and X. G. Gong, "Lattice-distortion induced magnetic transition from low-temperature antiferromagnetism to high-temperature ferrimagnetism in double perovskites A_2FeOsO_6 (A = Ca, Sr)," Sci. Rep. **5**, 13159 (2015).

[55]X. Z. Lu, X. Wu, and H. J. Xiang, "General microscopic model of magnetoelastic coupling from first principles," Phys. Rev. B **91**, 100405 (2015).
[56]Y. S. Hou, J. H. Yang, X. G. Gong, and H. J. Xiang, "Prediction of a multiferroic state with large electric polarization in tensile-strained $TbMnO_3$," Phys. Rev. B **88**, 060406 (2013).
[57]H. J. Xiang, P. S. Wang, M.-H. Whangbo, and X. G. Gong, "Unified model of ferroelectricity induced by spin order," Phys. Rev. B **88**, 054404 (2013).
[58]W. Zhong, D. Vanderbilt, and K. M. Rabe, "First-principles theory of ferroelectric phase transitions for perovskite: The case of $BaTiO_3$," Phys. Rev. B **52**, 6301–6312 (1995).
[59]L. Bellaiche, A. García, and D. Vanderbilt, "Finite-temperature properties of $Pb(Zr_{1-x}Ti_x)O_3$ alloys from first principles," Phys. Rev. Lett. **84**, 5427–5430 (2000).
[60]K. Chang, J. Liu, H. Lin, N. Wang, K. Zhao, A. Zhang, F. Jin, Y. Zhong, X. Hu, W. Duan, Q. Zhang, L. Fu, Q.-K. Xue, X. Chen, and S.-H. Ji, "Discovery of robust in-plane ferroelectricity in atomic-thick SnTe," Science **353**, 274–278 (2016).
[61]S.-W. Cheong and M. Mostovoy, "Multiferroics: A magnetic twist for ferroelectricity," Nat. Mater. **6**, 13–20 (2007).
[62]S. Dong, H. Xiang, and E. Dagotto, "Magnetoelectricity in multiferroics: A theoretical perspective," Nat. Sci. Rev. **6**, 629–641 (2019).
[63]J. S. Feng and H. J. Xiang, "Anisotropic symmetric exchange as a new mechanism for multiferroicity," Phys. Rev. B **93**, 174416 (2016).
[64]N. S. Fedorova, C. Ederer, N. A. Spaldin, and A. Scaramucci, "Biquadratic and ring exchange interactions in orthorhombic perovskite manganites," Phys. Rev. B **91**, 165122 (2015).
[65]X.-Y. Li, F. Lou, X.-G. Gong, and H. Xiang, "Constructing realistic effective spin Hamiltonians with machine learning approaches," New J. Phys. **22**, 053036 (2020).
[66]G. Carleo, I. Cirac, K. Cranmer, L. Daudet, M. Schuld, N. Tishby, L. Vogt-Maranto, and L. Zdeborova, "Machine learning and the physical sciences," Rev. Mod. Phys. **91**, 045002 (2019).
[67]J. Schmidt, M. R. G. Marques, S. Botti, and M. A. L. Marques, "Recent advances and applications of machine learning in solid-state materials science," npj Comput. Mater. **5**, 83 (2019).
[68]J. Behler, "Perspective: Machine learning potentials for atomistic simulations," J. Chem. Phys. **145**, 219901 (2016).
[69]A. Paszke, S. Gross, F. Massa, A. Lerer, J. Bradbury, G. Chanan, T. Killeen, Z. Lin, N. Gimelshein, L. Antiga, A. Desmaison, A. Kopf, E. Yang, Z. DeVito, M. Raison, A. Tejani, S. Chilamkurthy, B. Steiner, L. Fang, J. Bai, and S. Chintala, "PyTorch: An imperative style, high-performance deep learning library," in *Advances in Neural Information Processing Systems 322019*, edited by H. Wallach, H. Larochelle, A. Beygelzimer, F. d'Alche-Buc, E. Fox, and R. Garnett (NIPS, 2019).
[70]S. Ioffe and C. Szegedy, "Batch normalization: Accelerating deep network training by reducing internal covariate shift," in *Proceedings of the 32nd International Conference on Machine Learning, PMLR, Proceedings of Machine Learning Research*, edited by B. Francis and B. David (PMLR, 2015), pp. 448–456.
[71]B. A. Berg and T. Neuhaus, "Multicanonical algorithms for first order phase transition," Phys. Lett. B **267**, 249–253 (1991).
[72]A. P. Lyubartsev, A. A. Martsinovski, S. V. Shevkunov, and P. N. Vorontsov-Velyaminov, "New approach to Monte Carlo calculation of the free energy: Method of expanded ensembles," J. Chem. Phys. **96**, 1776–1783 (1992).
[73]K. Hukushima and K. Nemoto, "Exchange Monte Carlo method and application to spin glass simulations," J. Phys. Soc. Jpn. **65**, 1604–1608 (1996).
[74]U. H. E. Hansmann, "Parallel tempering algorithm for conformational studies of biological molecules," Chem. Phys. Lett. **281**, 140–150 (1997).
[75]Y. Miyatake, M. Yamamoto, J. J. Kim, M. Toyonaga, and O. Nagai, "On the implementation of the heat bath algorithms for Monte Carlo simulations of classical Heisenberg spin systems," J. Phys. C: Solid State Phys. **19**, 2539–2546 (1986).
[76]M. R. Hestenes and E. Stiefel, "Methods of conjugate gradients for solving linear systems," J. Res. Natl. Bur. Stand. **49**, 409–436 (1952).
[77]G. Kresse and J. Furthmüller, "Efficiency of *ab-initio* total energy calculations for metals and semiconductors using a plane-wave basis set," Comput. Mater. Sci. **6**, 15 (1996).
[78]G. Kresse and J. Furthmüller, "Efficient iterative schemes for *ab initio* total-energy calculations using a plane-wave basis set," Phys. Rev. B **54**, 11169 (1996).